

doi:10.3969/j.issn.1673-5374.2012.32.011 [http://www.crter.org/nrr-2012-qkquanwen.html]

Wu GY, Pang HP, Ghimire P, Liu GB. ¹H magnetic resonance spectroscopy and diffusion weighted imaging findings of medulloblastoma in 3.0T MRI: a retrospective analysis of 17 cases. *Neural Regen Res.* 2012;7(32):2554-2559.

¹H magnetic resonance spectroscopy and diffusion weighted imaging findings of medulloblastoma in 3.0T MRI

A retrospective analysis of 17 cases[☆]

Guangyao Wu, Haopeng Pang, Prasanna Ghimire, Guobing Liu

MR Room, Zhongnan Hospital of Wuhan University, Wuhan 430071, Hubei Province, China

Abstract

¹H magnetic resonance spectroscopy and diffusion weighted imaging features of the cerebellar vermis in 17 medulloblastoma patients were retrospectively analyzed, and 17 healthy volunteers were selected as controls. ¹H magnetic resonance spectroscopy showed that in all 17 medulloblastoma patients, N-acetyl aspartate and creatine peaks were significantly decreased, the choline peak was significantly increased, and there was evidence of a myo-inositol peak. Further, 11 patients showed a low taurine peak at 3.4 ppm, five patients showed a lipid peak at 0.9–1.3 ppm, and three patients showed a negative lactic acid peak at 1.33 ppm. Compared with the control group, the ratios of N-acetyl aspartate/choline and N-acetyl aspartate/creatine were significantly decreased, and the ratio of choline/creatine was increased, in medulloblastoma patients. Diffusion weighted imaging displayed hyperintensity and decreased apparent diffusion coefficient in medulloblastoma patients. These findings indicate that ¹H magnetic resonance spectroscopy and diffusion weighted imaging are useful for qualitative diagnosis of medulloblastoma.

Guangyao Wu[☆], M.D., Chief physician, MR Room, Zhongnan Hospital of Wuhan University, Wuhan 430071, Hubei Province, China

Corresponding author: Guangyao Wu, MR Room, Zhongnan Hospital of Wuhan University, Wuhan 430071, Hubei Province, China wuguangyao2002@yahoo.com.cn

Received: 2012-07-17
Accepted: 2012-10-22
(N20120213005/WJ)

Key Words

medulloblastoma; proton magnetic resonance spectroscopy; diffusion weighted imaging; apparent diffusion coefficient; N-acetyl aspartate; choline; creatine; taurine; lactic acid; myo-inositol

Research Highlights

- (1) 3.0T MRI features of 17 medulloblastoma patients were retrospectively analyzed.
- (2) ¹H magnetic resonance spectroscopy in combination with diffusion weighted imaging improved diagnostic accuracy of medulloblastoma.
- (3) Medulloblastoma patients showed a characteristic taurine peak and decreased apparent diffusion coefficient.

Abbreviations

MB, medulloblastoma; CSF, cerebrospinal fluid; ¹H MRS, proton magnetic resonance spectroscopy

INTRODUCTION

Medulloblastoma (MB) characterizes a neoplasm in the cerebellum of children, which exhibits rapid growth and originates

from an embryonic cell with the capability to differentiate into glial and neuronal cells. MB typically occurs between 5 to 10 years of age, and accounts for 25% of primary intracranial tumors in children, but only 1% in adults^[1]. MB prognosis is typically poor,

and relates to pathological type, onset age, biological behavior, postoperative residual lesion, cerebrospinal fluid spread, and hydrocephalus^[2-3]. MB can also disseminate through the cerebrospinal fluid in approximately 30% of firstly diagnosed MB patients^[4-5].

According to the 2007 World Health Organization classification of central nervous system neoplasms, MB is classified into five subtypes: classical, desmoplastic/nodular, extensive nodularity, anaplastic, and large cell MB^[6]. MB in children typically occurs in the cerebellum vermis, with a classical characteristic; while in adults, MB occurs in the cerebellum hemisphere, with a more desmoplastic/nodular pattern^[2, 7]. Furthermore, MBs are commonly stratified into standard risk and high risk groups based on onset age, pathological type, cerebrospinal fluid (CSF) disseminated or metastasis, and postoperative residual lesion (residual lesion > 1.5 cm²). To improve remission rates and the survival period, and to reduce the impact of radiotherapy on mental and cognitive function, standard risk MB is treated with maximum surgical resection followed by chemotherapy and whole brain radiotherapy (23.4 Gy in the craniospinal area plus a boost dose of 18–20 Gy in the posterior fossa). However, to improve the survival rate and prolong the survival period of high risk MB, treatment involves resection followed by continued chemotherapy of multi-drug combination and high dose radiotherapy (36 Gy in craniospinal area and a boost dose of 54 Gy in the posterior fossa)^[2-4]. Therefore, qualitative diagnosis of MB is crucial, including CSF

spread and other organ metastasis, and postoperative residual.

Proton magnetic resonance spectroscopy (¹H MRS) is a noninvasive method to detect changes in metabolites *in vivo*, while diffusion weighted imaging (DWI) is a valuable technique for probing the microscopic diffusion of water molecules. However, only a few reports have utilized these techniques to examine the histological features and biological behavior of MB. The present study aimed to retrospectively analyze ¹H MRS and DWI features of 17 MBs confirmed by pathology.

RESULTS

Quantitative analysis of participants

A total of 17 MB cases were selected, and 17 healthy volunteers were used as controls. All subjects were included in the final analysis.

Baseline data of participants

Baseline data of 17 MBs are listed in Table 1. In the series, 12 cases occurred in the cerebellar vermis (Figure 1A), four occurred in the cerebellar hemispheres, and one occurred in the right cerebellar hemisphere and vermis. Pathological typing indicated 11 classical MBs (Figure 2D), three desmoplastic/nodular MBs (Figure 1D), two large cell MBs, and one MB with extensive nodularity. There were also two cases with CSF spread (11.8%; Figure 1A).

Table 1 Clinical data of MB patients

Case	Gender	Age (year)	Clinical manifestation	Tumor position	Pathological subtype
1	Male	1.2	Irritability-restlessness, increasing head circumference anorexia	Cerebella vermis	Classic MB
2	Male	2.5	Headache papilledema	Cerebella vermis	Classic MB
3	Female	3.3	Headache instability of gait action clumsiness	Left cerebellar hemisphere	Classic MB
4	Female	9.4	Headache diplopia	Cerebella vermis	Desmoplastic/nodular MB
5	Male	4.6	Headache vomiting diplopia	Cerebella vermis	Classic MB
6	Female	5.7	Headache diplopia	Cerebella vermis	Classic MB
7	Male	6.4	headache vomiting diplopia	Cerebella vermis	MB with extensive nodularity
8	Female	7.2	Headache diplopia instability of gait	Right cerebellar hemisphere and vermis	Classic MB
9	Female	7.8	Headache diplopia	Cerebella vermis	Large cell MB
10	Male	8.3	Headache diplopia	Cerebella vermis	Classic MB
11	Male	3.9	Headache instability of gait	Left cerebellar hemisphere	Classic MB
12	Male	10.5	Headache vomiting diplopia	Cerebella vermis	Large cell MB
13	Male	11.7	Headache diplopia	Cerebella vermis	Classic MB
14	Female	12.1	Headache vomiting diplopia	Cerebella vermis	Desmoplastic/nodular MB
15	Male	18.6	Headache vomiting instability of gait	Left cerebellar hemisphere	Classic MB
16	Female	25.4	Headache diplopia instability of gait	Right cerebellar hemisphere	Desmoplastic/nodular MB
17	Male	35.6	Headache diplopia	Cerebella vermis	Classic MB

MB: Medulloblastoma.

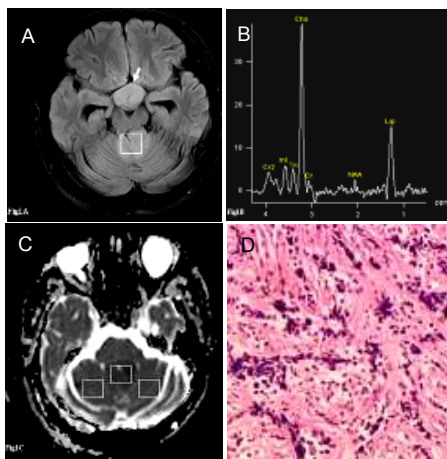


Figure 1 Case 4, female, 9 years old, with desmoplastic medulloblastoma in the cerebellar vermis accompanied by cerebrospinal fluid spread in the suprasellar cistern. The white squares represent the regions of interest used to select voxels to determine apparent diffusion coefficient values. The arrow represents a focus within the CSF in the suprasellar cistern.

(A) Transverse T2-fluid attenuated inversion recovery showing mild hyperintensity, CSF spread in suprasellar cistern (white arrow), and sv-PRESS localized in the center of the neoplasm (region of interest, $12 \times 12 \times 12 \text{ mm}^3$).

(B) ^1H MRS (repetition time/echo time = 1 500 ms/135 ms): the NAA and Cr peak was significantly decreased, and the Cho peak was significantly increased. There was an apparent taurine peak at 3.4 ppm and a myo-inositol peak at 3.56 ppm (X-axis: chemical shift, unit ppm; Y-axis: peak intensity of metabolite).

(C) ADC map: left square ADC value = 0.80, middle square ADC value = 0.62, right square ADC value = 0.84.

(D) Tumor morphology (hematoxylin-eosin staining, $\times 200$): desmoplastic medulloblastoma, with pale nodular areas surrounded by densely tumor cells, and rich reticulin. The tumor cells have more cytoplasm and a low rate of mitoses.

ADC: Apparent diffusion coefficient; Cho: choline; Cr: creatine; CSF: cerebrospinal fluid spread; NAA: N-acetyl aspartate; ^1H MRS: Proton magnetic resonance spectroscopy; sv-PRESS: single voxel point resolved spectroscopy technology.

All MB tumors showed well-defined margins and hypointensity on T1WI; 16 MBs showed hyperintensity, one showed isointensity on T2WI (Figures 1A, 2A), and three showed necrosis or cyst formation. Eight cases were complicated with hydrocephalus, and eight cases presented with obvious perifocal edema. In all 17 MBs, N-acetylaspartate (NAA) and creatine (Cr) peaks significantly decreased, choline (Cho) peak significantly increased, and there was evidence of a myo-inositol peak; DWI showed hyperintensity. Further, 11 MBs showed a low taurine peak at 3.4 ppm (accounting for 64.7%), five MBs showed a lipid peak at 0.9–1.3 ppm, and three MBs showed a negative lactic acid peak at

1.33 ppm (including one case with lipid and lactic acid peaks simultaneously).

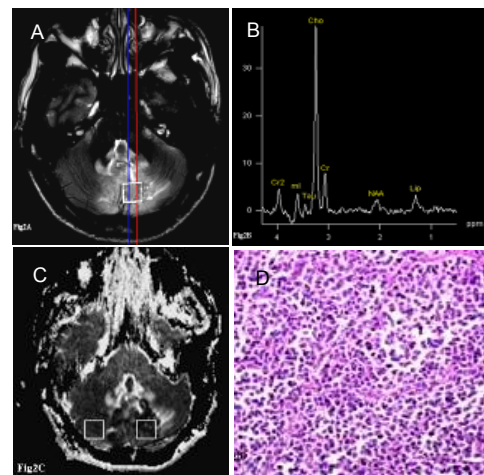


Figure 2 Case 13, male, 12 years old, with classic medulloblastoma in the cerebella vermis accompanied by cerebrospinal fluid spread in the suprasellar cistern.

The white squares represent regions of interest used to select voxels to determine ADC values.

(A) Transverse T2WI: slight hyperintensity, and sv-PRESS localized in the center of neoplasm (region of interest, $12 \times 12 \times 12 \text{ mm}^3$).

(B) ^1H MRS (repetition time/echo time = 1 500 ms/135 ms): NAA peak significantly decreased, Cr peak moderately decreased, Cho peak highly increased, low taurine peak at 3.4 ppm, and little myo-inositol peak.

(C) ADC map: Left square ADC value = 0.47, right square ADC value = 0.69.

(D) Tumor morphology (hematoxylin-eosin staining, $\times 200$): classic medulloblastoma, showing sheets of small, round cells with a high nucleus-to-cytoplasm ratio and abundant mitoses.

ADC: Apparent diffusion coefficient; Cho: choline; Cr: creatine; CSF: cerebrospinal fluid spread; NAA: N-acetyl aspartate; sv-PRESS: single voxel point resolved spectroscopy technology.

Table 2 Comparison of the metabolite ratios and apparent diffusion coefficient (ADC) between medulloblastoma and control groups

Item	Patient group (n = 17)	Control group (n = 17)	t
Mean ADC value ($\times 10^{-3} \text{ mm}^2/\text{s}$)	0.61 \pm 0.13	0.81 \pm 0.14 ^a	-4.332
NAA/Cho	0.13 \pm 0.05	1.18 \pm 0.24 ^a	-17.765
Cho/Cr	6.28 \pm 1.10	1.04 \pm 0.20 ^a	19.294

^a $P < 0.05$, vs. patient group (mean \pm SD, independent samples *t*-test). Data were obtained from the MRI workstation. Cho: Choline; Cr: Creatine; NAA: N-acetyl aspartate.

Compared with the control group, the ratios of NAA/Cho and NAA/Cr were significantly decreased, and the ratio of Cho/Cr was significantly increased ($P < 0.001$; Figures 1B, 2B, Table 2). The mean ADC value of MBs

was $0.61 \pm 0.13 \text{ mm}^2/\text{s}$, which was significantly decreased compared with the control group ($0.81 \pm 0.14 \text{ mm}^2/\text{s}$; $P < 0.001$; Figures 1C, 2C, Table 2). According to these findings, preoperative diagnoses for 17 MBs were all correct.

DISCUSSION

MB is an undifferentiated embryonal neuroepithelial tumor that commonly originates from multipotential neural progenitor cells in the external granular cell layer of the cerebellar vermis or cerebellar hemisphere^[3,5]. MB typically occurs in children from 5 to 10 years of age, with an incidence in Caucasians approximately 1.85 times that in Negros, and an incidence in males approximately 1.5 times that in females^[3,5]. The typical findings of MB are low or isointensity on T1WI, and high intensity on T2WI with various enhancements. Further, MB is disseminated through the CSF in approximately 30% of firstly diagnosed MB patients^[4]. In our series, there were two cases with CSF spread (11.8% of cases), while all cases corresponded to the typical features of MB on MRI. Nevertheless, it can be very difficult to distinguish between ependymoma and glioma types of MB in some cases.

We also found that ¹H MRS and DWI can improve the diagnostic accuracy of MB. ¹H MRS is a sensitive non-invasive method to detect the metabolic and biochemical changes in brain tumors. In our series, NAA and Cr peaks were significantly decreased, and the Cho peak was increased without the Ala peak at 1.47 ppm, corresponding to the ¹H MRS features of primitive neuroectodermal tumors^[8]. The causes of these metabolic changes may relate to neuronal cell death, cell proliferation and turnover of tumor cells, energy reserve decline in tumor cells, or propagation of glial cells^[8-9]. The absence of the Ala peak in MB is useful for distinguishing meningeoma^[8]. A previous study reported that the myo-inositol peak was more common in MBs with long TE PRESS, but rarely observed in high grade glioma and lymphoma, indicating that the myo-inositol peak may be a characteristic peak in MB^[8]. In addition, five MBs showed a lipid peak at 0.9–1.3 ppm, and three MBs showed a negative lactic acid peak at 1.33 ppm, which may have resulted from apoptosis and necrosis of tumor cells, or turnover of tumor cells; however, this finding may also occur in high-grade glioma and lymphoma. Nevertheless, the predominant feature of MB on 1H MRS was reported to be a taurine peak at 3.4 ppm^[2,8]. In our series, 11 MBs showed a low taurine peak in 64.7% of subjects. Moreno-Torres^[10] reported that MB cases could be

detected using taurine in stimulated echo acquisition mode (echo time, 20 ms), while astrocytomas could not be detected. These contrasting results may relate to the different echo times used in these studies. Several studies have reported detection of a taurine peak in renal carcinoma, colon cancer, astrocytoma, and pinealoma samples with high resolution ¹H MRS, although taurine peaks could not be detected in any normal cerebellar tissue, suggesting that the taurine peak is characteristic of MB *in vivo*^[11-13].

Taurine is a β -amino acid. It is highly expressed in fetal neural tissues, and then gradually decreases during postnatal development, to reach adult levels at approximately weaning age^[10, 14]. The functions of taurine include neuroprotection, neuro-modulation, cell migration, and development in the central nervous system^[15-17]. These functions are mediated through effective removal of hypochlorous acid in tissues, modulation of calcium levels, maintenance of osmolarity, and stabilization of membranes. In addition, taurine may play a neuroprotective role by interacting with gamma-aminobutyric acid A receptors and counteraction of central nervous system cell toxicity. The taurine peak may also act as a biological marker of early large cell or anaplastic MB with more aggressiveness and poor prognosis^[10]. Further, desmoplastic MB or MB with extensive nodularity showed a lower aggressiveness and better prognosis, with a lower taurine concentration, than those of large cell or anaplastic MBs^[12, 18-19]. Overall, these data suggest that taurine concentration may be useful for detection of specific subtypes and biological behaviors of different types of MB. Peet *et al*^[20] reported that MB with metastasis showed higher taurine concentration than MB without metastasis. Our data also support that the taurine peak is a biomarker of MB.

DWI has been widely used to study cerebral infarction, multiple sclerosis, tumors, abscesses, and other intracranial diseases. For example, ADC values can change in response to tumor hypercellularity^[21]. In our present series, all 17 MBs showed hyperintensity on DWI and decreased ADC (mean ADC, $0.61 \pm 0.13 \times 10^{-3} \text{ mm}^2/\text{s}$; range $0.39\text{--}0.78 \times 10^{-3} \text{ mm}^2/\text{s}$). This relatively restricted diffusion of water molecules may relate to high tumor cellularity, reduction in extracellular space, reduction in extent of water molecule diffusion, or a reduction in dephasing of water molecule. A relatively hyperintense DWI signal of the MB parenchyma compared with that of the normal brain parenchyma was also reported^[21-22]. Posterior fossa tumors typically include MB, cerebellar astrocytoma, ependymocytoma, and brain-stem glioma,

accounting for more than 95% of childhood tumors in the area. In contrast to MB, the cerebellar astrocytoma, ependymocytoma, and brain-stem glioma often show hypointensity on DWI and an increase in ADC. Thus, DWI features and quantitative ADC analysis may help to determine the preoperational grade of cerebellar astrocytoma or ependymoma^[21-22]. Gauvain *et al*^[21] reported that MB was hyperintense on DWI, with a decreased ADC (mean ADC, $0.72 \pm 0.2 \times 10^{-3} \text{ mm}^2/\text{s}$; range $0.538\text{--}0.974 \times 10^{-3} \text{ mm}^2/\text{s}$), while high-grade glioma exhibited DWI hypointensity and increased ADC (mean ADC, $1.22 \pm 0.09 \times 10^{-3} \text{ mm}^2/\text{s}$; range $1.128\text{--}1.303 \times 10^{-3} \text{ mm}^2/\text{s}$); there was a significant difference in ADC between the types of MB ($P < 0.05$). Rumboldt *et al*^[22] reported that DWI could distinguish between pilocytic astrocytoma, MB, and ependymoma, with an increased ADC in pilocytic astrocytoma and ependymoma (mean ADC, $1.65 \pm 0.27 \times 10^{-3} \text{ mm}^2/\text{s}$ and $1.10 \pm 0.11 \times 10^{-3} \text{ mm}^2/\text{s}$, respectively), and a decreased ADC in MB (mean ADC, $0.66 \pm 0.15 \times 10^{-3} \text{ mm}^2/\text{s}$); the differences between MB, pilocytic astrocytoma, and ependymoma were significant^[22]. Fruehwald-Pallamar *et al*^[6] also reported a decrease in ADC in MB (mean ADC, $0.678 \times 10^{-3} \text{ mm}^2/\text{s}$; range $0.42\text{--}0.87 \times 10^{-3} \text{ mm}^2/\text{s}$). However, the ADC value range in that study was not totally consistent with other reports, which may relate to differences in sample size, proportion of MB subtypes, main magnetic field strength, position of ROI, and the *b* value.

In conclusion, ¹H MRS is useful for detection of metabolic abnormalities and biochemical changes in MB. In particular, taurine is a potential biomarkers of MB on ¹H MRS. The characteristic ¹H MRS and DWI findings of MBs may be useful to improve their diagnostic accuracy, while qualitative analysis of the taurine peak, and quantitative analysis of ADC, allow detection of the biological behavior and prognosis estimation of MB, as well as the choice of therapeutic schedule.

SUBJECTS AND METHODS

Design

A retrospective case analysis.

Time and setting

The experiment was performed in the Zhongnan Hospital of Wuhan University, China from April 2009 to November 2011.

Subjects

A total of 17 MB patients confirmed by pathology were

collected from Zhongnan Hospital of Wuhan University, China from April 2009 to November 2011, including 10 males and seven females (average age of onset, 10.0 ± 8.9 years; range 1.2–35.6 years). In addition, 17 healthy, age- and gender-matched volunteers, who were negative for conventional MRI, were selected as controls, and their monomer ¹H MRS was collected at the same site in patients. Inclusion criteria: clinical data was complete; all cases were confirmed by post-surgical pathology with clear pathological subtype (classical, desmoplastic/nodular, extensive nodularity, anaplastic, and large cell MB); all cases had high-quality ¹H MRS, DWI, and conventional scan data.

Methods

MRI protocol

Brain MRI, ¹H MRS, and DWI sequences were performed with a 3.0T MRI unit (Magnetom Tim Trio; Siemens Medical Solutions, Erlangen, Germany). MRI plain scan included transverse T1-FLAIR (repetition time (TR)/echo time (TE)/inversion time (TI), 2 000 ms/9.1 ms/860 ms); T2-FLAIR (TR/TE/TI, 9 000 ms/93 ms/2 500 ms); sagittal T1-FLASH (TR/TE/Flip angle, 400 ms/2.8 ms/90°); enhancement scan included transverse/sagittal/coronal T1-FLAIR (TR/TE/TI, 2 000 ms/9.1 ms/860 ms); thickness/gap, 5 mm/1 mm; field of view 240 × 240 mm; matrix, 256 × 384. ¹H MRS and DWI were performed prior to enhancement scan. A single voxel of ¹H MRS localized the solid part of the MBs and avoided areas of necrosis using a point resolved selective spectroscopy sequence (PRESS, TE/135 ms, TR/1 500 ms; voxel volume, 12 × 12 × 12 mm; number of averages, 128). DWI was used to scan the entire brain (spin-echo echo planar imaging; *b* values, 0 and 1 000 s/mm²).

Imaging evaluation

The imaging data from all patients were double-blind assessed by two neuroradiologists to reach consensus as a standard. These findings, including neoplasm solid, necrosis, edema, and enhancement, were described on plain and enhanced pictures. Post-processing and analysis of ¹H-MRS and DWI data were performed with Siemens independent workstation (version, syngo B17). On ¹H MRS, the following metabolites peaks and their ratios were evaluated: NAA (2.02 ppm), Cho (3.22 ppm), Cr (3.03 ppm), taurine (3.42 ppm), myo-inositol (3.56 ppm), lipid (0.9–1.3 ppm), and lactic acid (1.33 ppm). The ratios of NAA/Cho, NAA/Cr, and Cho/Cr, and the ADC values of MBs, were compared with the control group by independent samples *t*-test. ADC values were measured in 240 × 240 mm² ROI. Postoperative specimens were subjected to hematoxylin-eosin staining.

Statistical analysis

Statistical analysis was performed in 13.0 SPSS software (SPSS, Chicago, IL, USA). Semi-quantitative metabolite ratios and quantitative ADC values were analyzed by independent samples *t*-test. A value of *P* < 0.05 was considered statistically significant.

Funding: This study was supported by the National Natural Science Foundation of China, No. 81171315; the Fundamental Research Funds of the Central Universities, No. 303275894; and the Natural Science Foundation of Hubei Province, No. 2009CDA071.

Author contributions: Guangyao Wu was responsible for study design, data analysis, literature search, and paper writing. Haopeng Pang participated in the study design and data analysis. Prasanna Ghimire was in charge of data analysis and manuscript supervision. Guobin Liu provided the technical support.

Conflicts of interest: None declared.

Author statements: The manuscript is original, has not been submitted to or is not under consideration by another publication, has not been previously published in any language or any form, including electronic, and contains no disclosure of confidential information or authorship/ patent application disputations.

REFERENCES

- [1] Mcneil DE, Cote TR, Clegg L, et al. Incidence and trends in pediatric malignancies medulloblastoma/primitive neuroectodermal tumor: a seer update. *Med Pediatr Oncol*. 2002;399(3):190-194.
- [2] Brandes AA, Paris MK. Review of the prognostic factors in medulloblastoma of children and adults. *Crit Rev Oncol Hematol*. 2004;50(2):121-128.
- [3] Dhall G. Medulloblastoma. *J Child Neurol*. 2009;24(11):1418-1430.
- [4] Gilbertson RJ. Medulloblastoma: signalling a change in treatment. *Lancet Oncol*. 2004;5(4):209-218.
- [5] Fruehwald-Pallamar J, Puchner SB, Rossi A, et al. Magnetic resonance imaging spectrum of medulloblastoma. *Neuroradiology*. 2011;53(6):387-396.
- [6] Louis DN, Ohgaki H, Wiestler OD, et al. The 2007 WHO classification of tumours of the central nervous system. *Acta Neuropathol*. 2007;114(2):97-109.
- [7] Furtado SV, Venkatesh PK, Dadlani R, et al. Adult medulloblastoma and the "dural-tail" sign: rare mimic of a pos-terior petrous meningioma. *Clin Neurol Neurosurg*. 2009;111(6):540-543.
- [8] Jouanneau E, Guzman TR, Desuzinges C, et al. Very late frontal relapse of medulloblastoma mimicking a meningioma in an adult: usefulness of 1H magnetic resonance spectroscopy and diffusion-perfusion magnetic resonance imaging for preoperative diagnosis: case report. *Neurosurgery*. 2006;58(4):E789.
- [9] Lindskog M, Kogner P, Ponthan F, et al. Noninvasive estimation of tumour viability in a xenograft model of human neuroblastoma with proton magnetic resonance spectroscopy (1H MRS). *Br J Cancer*. 2003;88:478-485.
- [10] Moreno-Torres A, Martinez-Perez I, Baquero M, et al. Taurine detection by proton magnetic resonance spectroscopy in medulloblastoma: contribution to noninvasive differential diagnosis with cerebellar astrocytoma. *Neurosurgery*. 2004;55(4):824-829.
- [11] Chawla A, Emmanuel JV, Seow WT, et al. Paediatric PNET: pre-surgical MRI features. *Clin Radiol*. 2007;62(1): 43-52.
- [12] Salunke P, Gupta K, Kovai P, et al. Preoperative diffuse leptomeningeal spread in a medulloblastoma: Paraplegia following surgery for posterior fossa and call for newer management protocols. *J Pediatr Neurosci*. 2011;6(2): 152-154.
- [13] Tong ZY, Yamaki T, Harada K, et al. In vivo quantification of the metabolites in normal brain and brain tumors by proton MR spectroscopy using water as an internal standard. *Magn Reson Imaging*. 2004;22(7):1017-1024.
- [14] Hekmatyar SK, Wilson M, Jerome N, et al. 1H nuclear magnetic resonance spectroscopy characterisation of metabolic phenotypes in the medulloblastoma of the SMO transgenic mice. *Br J Cancer*. 2010;103(8):1297-304.
- [15] Timbrell JA, Seabra V, Waterfield CJ. The in vivo and in vitro protective properties of taurine. *Gen Pharmacol*. 1995;26(3):453-462.
- [16] Kramer K, McCrea HJ, Fischer C, et al. Establishing successful cerebrospinal fluid flow for radioimmunotherapy. *J Neurosurg Pediatr*. 2012;9(3): 316-319.
- [17] Albrecht J, Schousboe A. Taurine interaction with neurotransmitter receptors in the CNS: an update. *Neurochem Res*. 2005;30(12):1615-1621.
- [18] Davies NP, Wilson M, Harris LM, et al. Identification and characterisation of childhood cerebellar tumours by in vivo proton MRS. *NMR Biomed*. 2008;21(8):908-918.
- [19] Mcmanamy CS, Pears J, Weston CL, et al. Nodule formation and desmoplasia in medulloblastomas - Defining the nodular/desmoplastic variant and its biological behavior. *Brain Pathol*. 2007;17(2):151-164.
- [20] Peet AC, Davies NP, Ridley L, et al. Magnetic resonance spectroscopy suggests key differences in the metastatic behaviour of medulloblastoma. *Eur J Cancer*. 2007;43(6): 1037-1044.
- [21] Gauvain KM, Mckinstry RC, Mukherjee P, et al. Evaluating pediatric brain tumor cellularity with diffusion-tensor imaging. *AJR Am J Roentgenol*. 2001;177(2):449-454.
- [22] Rumboldt Z, Camacho DL, Lake D, et al. Apparent diffusion coefficients for differentiation of cerebellar tumors in children. *AJNR Am J Neuroradiol*. 2006;27(6):1362-1369.

(Edited by Miao YW, Wang XL/Su LL/Song LP)